Reconstructing Parent Microstructures in Martensitic and Pearlitic Ti-Cu

Alec I. Saville[1], Amy J. Clarke[1]

Colorado School of Mines[1], 1500 Illinois Street, Golden, CO, 80401

Corresponding author: Alec Saville, alec.saville@gmail.com, 303-990-0939

Abstract

Evaluating the microstructural evolution of parent phases has long been a challenge in metals with a partial or complete solid-state transformation. Most parent microstructure evolution has to be inferred from the product microstructure, with some information permanently lost. Parent microstructure reconstructions relying on orientation relationships and EBSD data are a useful tool to overcome this challenge, though much background knowledge is required to do so. This work introduces a reconstruction process for a eutectoid composition Ti-Cu binary alloy to evaluate the high temperature β-Ti phase from martensitic and pearlitic product microstructures. Martensitic microstructures were accurately reconstructed, enabling elucidation of β-Ti grain size and texture, and the employed script included for scientific reference. Eutectoid microstructures did not reconstruct effectively with the current process. However, new insight into the interfacial crystallographic orientations of lamellae Ti-Cu microstructures was gleaned via this analysis, and future investigations of interest are discussed accordingly. Ultimately, these findings demonstrate tools widely implemented on conventional titanium and ferrous alloys can also be applied to understand parent microstructures in Ti-Cu and other alloys of emerging interest. This is especially of use as new manufacturing processes for such materials require understanding how parent phase microstructures respond to new, novel material processing such as AM.

1 Introduction

The reconstruction of parent microstructures in metallic systems is a tool widely employed to gain knowledge about the orientation, size, and history of a parent phase prior to partial or complete solid state transformation. Such information can inform how processing with different conditions (e.g., at high temperatures) alters the stable phase, and consequently influences the transformed product microstructure. Examples of reconstruction applications include the calculation of parent austenite grains from martensite for grain size estimation [1,2] parent β-Ti grains from an additively manufactured (AM) Ti-6Al-4V build for texture and grain size [3–5], and the determination of parent grain orientations from low symmetry martensite to predict shape memory effect deformation structures in uranium alloys [6,7]. Parent phase reconstructions are often employed for titanium- and iron-based alloys considering the numerous solid-state transformations present in these systems.

Parent microstructure reconstructions require spatially resolved orientation data and knowledge about an expected or estimated orientation relationship (OR) between the parent and product phases. Electron backscatter diffraction (EBSD) data is widely used to acquire this spatially resolved orientation data. Tools such as ARPGE [8,9], TIBOR [10], and MTEX [11] are employed to carry out the reconstruction process through a multitude of different voting processes, while add-ons such as ORTools [1] can help identify suitable OR's and misorientations within a given

dataset. The development of multiple open-access tools for parent microstructure reconstructions has expanded the application space for using such calculations in metallurgical investigations, consistently building off of previous improvements in computational segmentation and crystallographic data processing [1,2,8–13]. This has opened new avenues for characterizing solid-state microstructural conditions after the parent phase has partially or fully transformed.

One such direction of recent work has been the exploration of solid-state transformations in metal alloys of emerging interest. Ti-Cu binary alloys have gained attention in the additive manufacturing (AM) and biomedical fields for producing fine-grained as-built microstructures with excellent strength [14] and desirable antimicrobial/biological properties [15–18]. When cooled rapidly from the high temperature β-Ti regime, Ti-Cu takes on a fully α' martensitic microstructure [19,20]. When cooled slowly, a pearlitic eutectoid structure of α-Ti + Ti_2Cu forms [19]. Intermediate cooling rates can form microstructures analogous to upper bainite in steels [21]. All three microstructures are of engineering interest for application specific properties akin to that in ferrous alloys, but little can be inferred on how processing of the high temperature β-Ti phase impacts the lower temperature microstructure development. To better understand this as Ti-Cu expands into engineering applications in AM, dentistry, and antimicrobial applications, EBSD and parent phase reconstruction is required. This work evaluates the effectiveness of reconstructing Ti-Cu parent β-Ti microstructures as this alloy system gains prominence in engineering applications.

Williams et al. [20] previously reported Ti-Cu α' martensite exhibits the Burgers OR, $\{0001\}_\alpha \parallel \{110\}_\beta$ and $\{11\bar{2}0\}_\alpha \parallel \{111\}_\beta$, with the parent β-Ti phase but this has yet to be tested in reconstruction processes. Due to the single-phase nature of the martensitic microstructure, reconstruction of the parent β-Ti phase should be simpler than that for multi-phase microstructures. ORs for the dual phase $\alpha + Ti_2Cu$ eutectoid microstructure have not been identified to the authors best knowledge for eutectoid Ti-Cu compositions, and is an area for future investigations.

Such determination is not trivial however, considering three ORs are likely present in eutectoid lamellae microstructures: that between the α-Ti and Ti_2Cu, that between α-Ti and β-Ti, and that between Ti_2Cu and β-Ti. This is similar to the ORs observed for the pearlite microconstituent in ferrous alloys [22]. It stands to reason the α-Ti and β-Ti may still take on a Burgers OR in the eutectoid microstructure, and may be used to approximate the reconstructed parent β-Ti phase.

Previous work on hypereutectoid 12 at% Cu (~15 wt%) binary Ti-Cu identified an OR between β-Ti and Ti_2Cu as $[001]_{Ti_2Cu} \parallel < 001 >_\beta$, $[100]_{Ti_2Cu} \parallel < 100 >_\beta$, and $[010]_{Ti_2Cu} \parallel < 010 >_\beta$ and an OR between α-Ti and Ti_2Cu as $\{0\bar{1}3\}_{Ti_2Cu} \parallel \{0001\}_\alpha$ and $\{331\}_{Ti_2Cu} \parallel \{11\bar{2}0\}_\alpha$. These ORs held in both blocky (phase nucleation along boundaries) and in lamellar microstructures [23]. The Burgers OR was also reported to dominate the orientation between α-Ti and β-Ti in both microstructures. However, these ORs have not been confirmed in eutectoid compositions for Ti-Cu binaries with nearly half the copper content. If they do hold however, they may enable the recalculation of parent microstructures from pearlitic microstructures as well as those consisting of α' martensite.

As such reconstructions have not been completed to date, this work explores the accuracy and validity of parent β-Ti microstructure reconstructions using the open-access MTEX tool for both martensitic and pearlitic product microstructures in a eutectoid composition Ti-Cu binary alloy containing 7.53 wt% Cu. Bainitic Ti-Cu microstructures are not included in this work given both

martensitic and eutectoid dominated portions of the microstructure can exist, complicating the reconstruction process [21,24,25].

2 Materials and Methods

2.1 Sample Production and Metallographic Prep

Dilatometry specimens of Ti-7.53 wt% Cu were heat treated using a DIL 805L dilatometer to create martensitic and eutectoid microstructures for evaluating parent β-Ti reconstructions. These specimens consisted of 4 mm x 10 mm x 1.75 mm sheet sections of the binary Ti-Cu alloy, and contained a fully pearlitic eutectoid microstructure to start. Both specimens were heated above the eutectoid temperature (~ 800 °C) at 55 °C/sec and held at 850 °C for 30 sec to establish β-Ti grains. All temperatures were measured via S-type thermocouples attached to the center of the specimen's surface. The eutectoid transformation temperature for this system is estimated to be ~ 800 °C, above which β-Ti will nucleate and consume the eutectoid microstructure. Cooling below this temperature at different cooling rates will produce different product microstructures [19]. The martensitic specimen was quenched to room temperature with a 500 °C/sec cooling rate with helium gas. Another specimen was helium cooled to 600 °C at 55 °C/sec, held for 15 seconds, and then helium gas quenched at 500 °C/sec to prevent further microstructural evolution and produce a eutectoid microstructure. It is important to note both specimens were expected to have *the same parent β-Ti grain size* from the identical trans-eutectoid heat treatments. Both specimens were metallographically prepared using 800 grit sand paper, 9 μm and 6 μm diamond solutions, and 0.05 μm colloidal silica. Etching of the polished samples was achieved with 25 mL of deionized water and 5 mL of hydrofluoric acid.

2.2 Microscopy and EBSD

Light optical micrographs using differential interference contrast and polarized light were captured using an Olympus 500X to characterize the etched microstructures. Estimation of parent grain sizes from the etched microstructure was completed using the Abrams Concentric Circle method according to ASTM [26]. Backscatter electron micrographs were captured using a Tescan S8000 scanning electron microscope (SEM) for higher resolution imaging with 20 keV accelerating voltage and 3 nA probe current. EBSD maps were collected using a FEI Helios Nanolab 600I FIB/SEM equipped with an EDAX "Hikari Super" EBSD Detector with 20 keV accelerating voltages and 11 nA probe currents. EBSD mapping of both specimens was completed with 0.2 μm and 0.5 μm step sizes for the martensite and lamellae microstructures respectively. In order to capture sufficient data to capture multiple parent β-Ti grains, maps of ~ 400 μm x 400 μm area were acquired.

2.3 Processing EBSD Data

All EBSD data was processed using MTEX 5.70 in MATLAB R2020b. No processing was applied to the datasets prior to loading into MTEX.Discretegrains were calculated using a threshold of 5° within each inverse pole figure (IPF) map. Pole figures in this work were created with orientation distribution functions (ODFs) in MTEX using a 5° resolution. β-Ti reconstruction from the α' martensite and eutectoid microstructure was completed using MTEX 5.70's graph method and the Burgers OR to relate product-to-parent orientations [1,13]. The martensite reconstruction script employed for this work is included as part of the supplementary materials as reference for other researchers in future and related investigations. Discussion of how this reconstruction process

operates has already been documented in literature, and was not the focus of this work [13]. A unique triple point calculation process was also applied to recalculate the parent grain structure from eutectoid EBSD data [1].

3 Results and Discussion

3.1 Light Optical Microscopy

Prior to reconstructing the parent grain structures of both the eutectoid and martensitic microstructures, the solid state microstructures were initially surveyed. The etched martensitic microstructure observed in Figure 1a highlights the parent β-Ti grains, giving a clear estimate of what the reconstructed β-Ti grain sizes should be for this condition (~ 75 μm). Etched eutectoid microstructures illustrate partial remnant β-Ti grain boundaries of comparable size, and under polarized light reveal uniquely oriented α-Ti + Ti_2Cu colonies. In contrast to pearlite colonies in ferrous alloys [27], α-Ti + Ti_2Cu colonies appear to both grow from parent grain boundaries into prior β-Ti grains and also across parent grain boundaries from an unspecified nucleation point internal to other parent β-Ti grains (Figure 1b). The mechanisms and origins of this behavior are recommended for future investigations, and explain the complex microstructures observed in Figure 1c. Regardless, the remnant grain boundaries outline parent grains comparable to those seen in the etched martensite microstructures (~ 75 μm). This validated that both trans-eutectoid heat treatments produced the same parent grain sizes, establishing a known value to expect from β-Ti reconstructions.

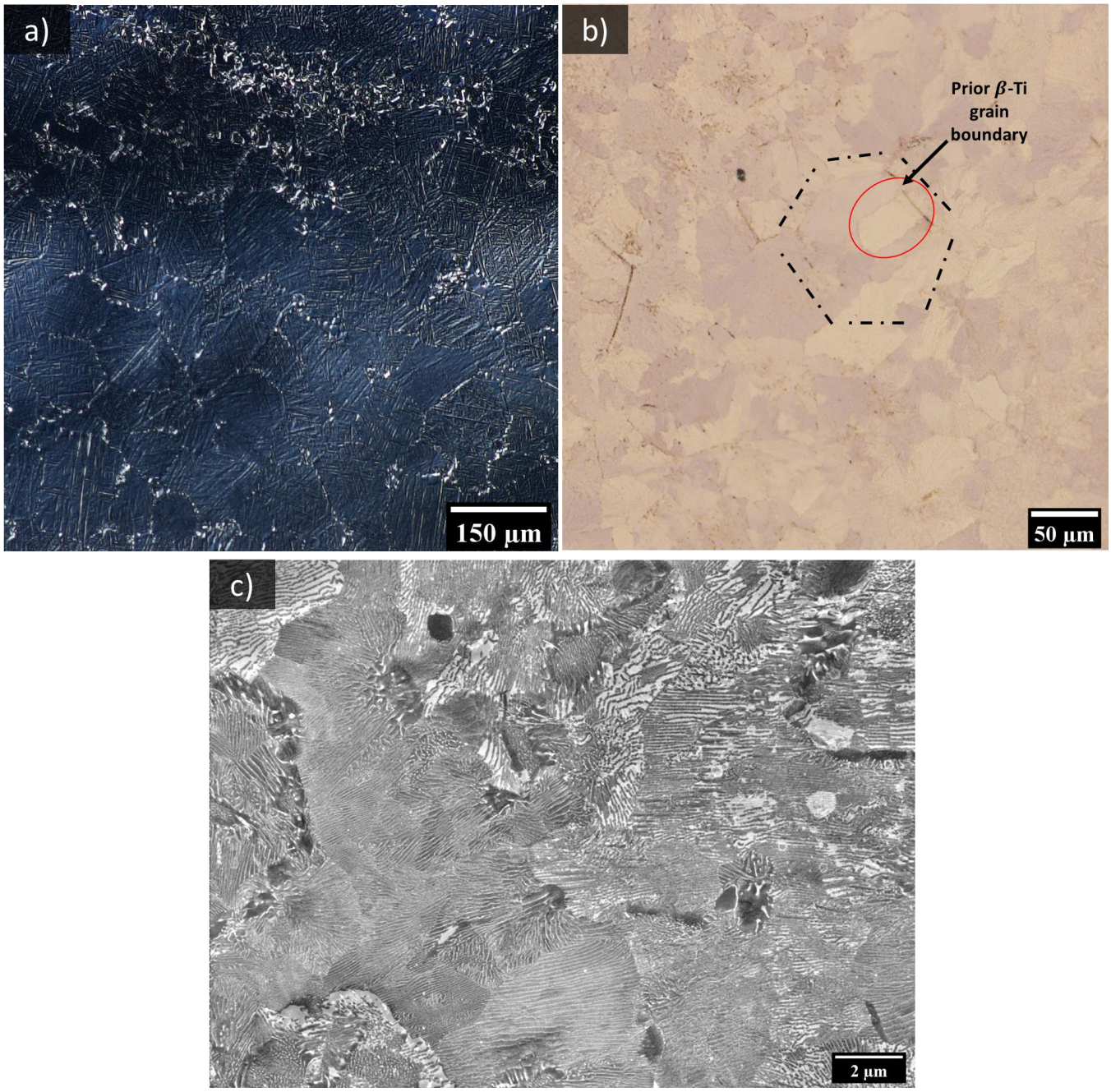

Figure 1: a) Light optical micrograph of α' martensite within prior β-Ti parent grains outlined after 500 °C/sec cooling from the β-Ti phase field. Image contrast is supplied by differential interference contrast. The average β-Ti grain size was about ~ 75 μm as observed by the etched grain boundaries. b) Polarized light micrograph of an etched Ti-Cu eutectoid microstructure illustrating prior β-Ti grain boundaries and different crystallographic orientations of unique α-Ti + Ti_2Cu eutectoid colonies. The red circle outlines a colony suspected of growing through a parent β-Ti grain boundary in contrast to traditional pearlitic nucleation and growth mechanisms [27]. This is suggested by the nearby colony growing across the remnant grain boundary. A faint outline of the parent β-Ti grain boundary can be seen in the black dashed-line region. The estimated parent β-Ti grain size is comparable to that seen in a) at ~ 75 μm, validating the trans-eutectoid heat

treatments produced the same parent microstructures. c) Backscatter electron scanning electron micrograph of eutectoid α-Ti + Ti_2Cu lamellae microstructure.

3.2 EBSD of α' Martensite

EBSD of the α' martensitic microstructure is demonstrated in Figure 2, with the parent β-Ti grain size evident from the different martensite variants. Some eutectoid α-Ti + Ti_2Cu may exist at prior β-Ti grain boundaries as evidenced by the globular clusters of orientations outlining some parent grains. This confirms previous investigations which found the α-Ti + Ti_2Cu microstructure forms rapidly as an active eutectoid, requiring considerably rapid cooling to fully suppress [19].

The raw orientation data acquired in Figure 2a includes many ultrafine martensitic lathes unable to be resolved visually in the dataset when using an MTEX misorientation of 5° to define separate grains. Thus, the martensitic orientation data was filtered by removing grains less than three pixels in total and growing nearby grains into the now empty volume (Figure 2b). This process was shown to have a minimal negative effect on the solid-state reconstruction process as long as enough other product orientations are left over in each parent grain. Thus, the filtered α' data in Figure 2b was implemented for reconstruction of the parent microstructure.

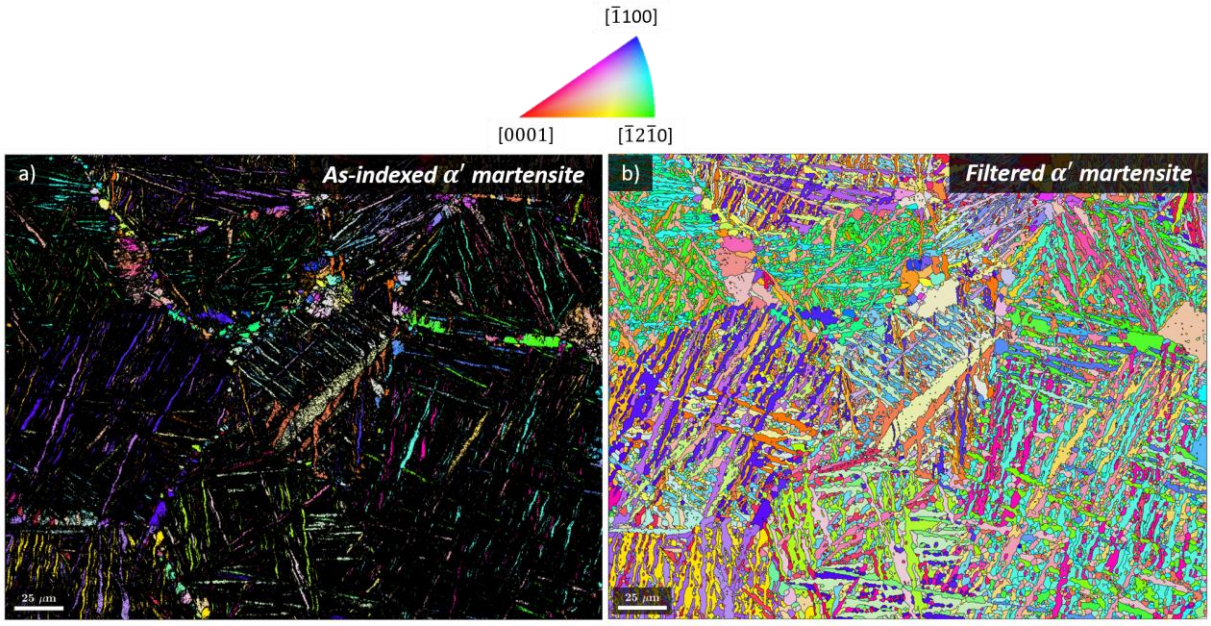

Figure 2: a) Raw α' martensite IPF map for the eutectoid Ti-Cu alloy. b) A filtered, mean grain orientation IPF map of the α' martensite EBSD data in a) after removing small grains to reduce the computational loading of the reconstruction process. Both maps are colored with respect to the normal direction (out of the screen).

Evaluation of the grain-to-grain misorientations demonstrates a significant preference for the martensite to crystallographically orient ~ 63° apart, suggesting a favorable misorientation is present during the martensitic transformation in this Ti-Cu alloy. Both histogram and overlaid misorientation maps demonstrate the ubiquity of this misorientation (Figure 3). Crystallographically, this misorientation corresponds to the $(10\bar{1}0) \,||\, (10\bar{1}0)$ planes and the

[0001] || [0001] directions of each martensite lath aligning parallel to one another across the grain boundary interface. With this information it may be possible to identify the habit plane of α' with β-Ti if the parent orientation is known, but this is the subject of future work. Past work has suggested a number of candidates, but no single habit plane has been agreed upon [20].

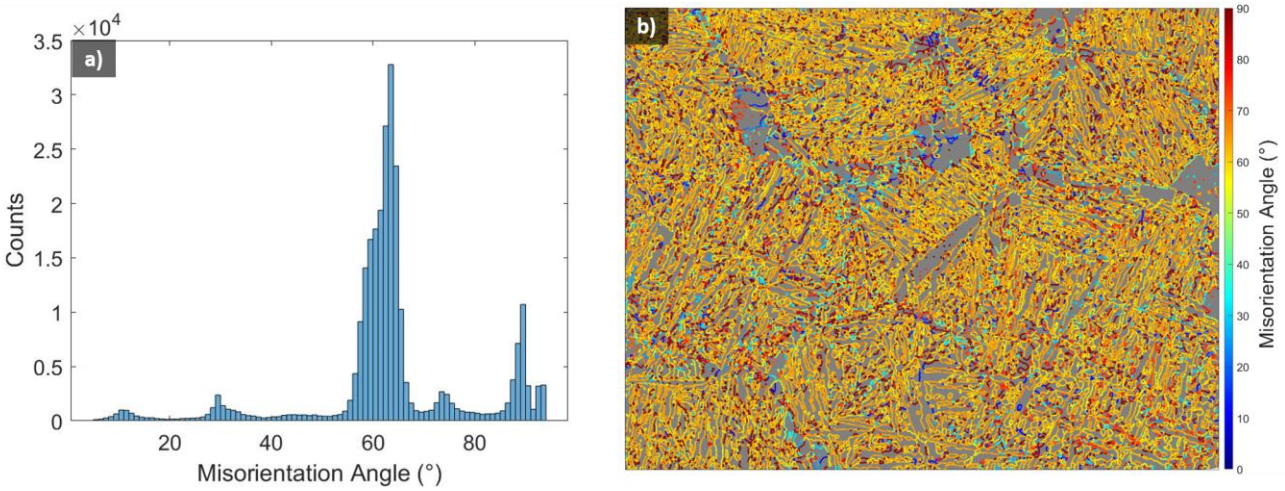

Figure 3: a) Misorientation angle histogram for martensite-martensite boundaries illustrating a favorable misorientation at ~ 63°. b) Martensite-martensite angular misorientation spatially overlaid on α' grain boundaries.

3.3 Reconstructing β-Ti Microstructures from α' Martensite

Implementing MTEX's variant graph method to reconstruct the β-Ti grains produces the orientation map observed in Figure 4a. By quick comparison of Figure 4a and Figure 2a, it can be seen the reconstruction process was fairly successful in identifying discrete parent β-Ti grains by using the Burgers OR. Overlaying the recalculated parent β-Ti grains on the product microstructure (Figure 4b) additionally demonstrates this good fitting to the parent grain boundaries evident in Figure 2. This confirms the α' martensite exhibits a Burgers OR with the parent phase as reported by Williams et al. [20], enabling the reconstruction of the β-Ti phase for Ti-Cu. It is worth noting the parent grain boundaries in Figure 4 are not exact. These boundaries are approximations calculated during the reconstruction process, and can be improved with subsequent smoothing and other processes [1,13]. Such operations were not carried out here besides the filling of low-pixel count holes to illustrate the raw output of this reconstruction process.

Visualizing the crystal orientations (Figure 4c) for the reconstructed microstructure demonstrates a preference for the $(111)_\beta$ to orient along the normal direction (out of the page), potentially indicative of rolling operations applied during production of the sheet feedstock used in this study. This confirms previously hidden information about the parent microstructure can be ascertained via this reconstruction process using existing capabilities. Such a capability has not been demonstrated for Ti-Cu to date, and evaluating if such insight can be determined for this alloy system is one of the core objectives for this work. The overlap of the $(0001)_\alpha$ -- $(110)_\beta$ and the $(11\bar{2}0)_\alpha$ -- $(111)_\beta$ pole figures (Figure 4d) additionally confirm the Burgers OR dominates the crystallographic configuration of the material and enables the *accurate* reconstruction of the parent β-Ti microstructure.

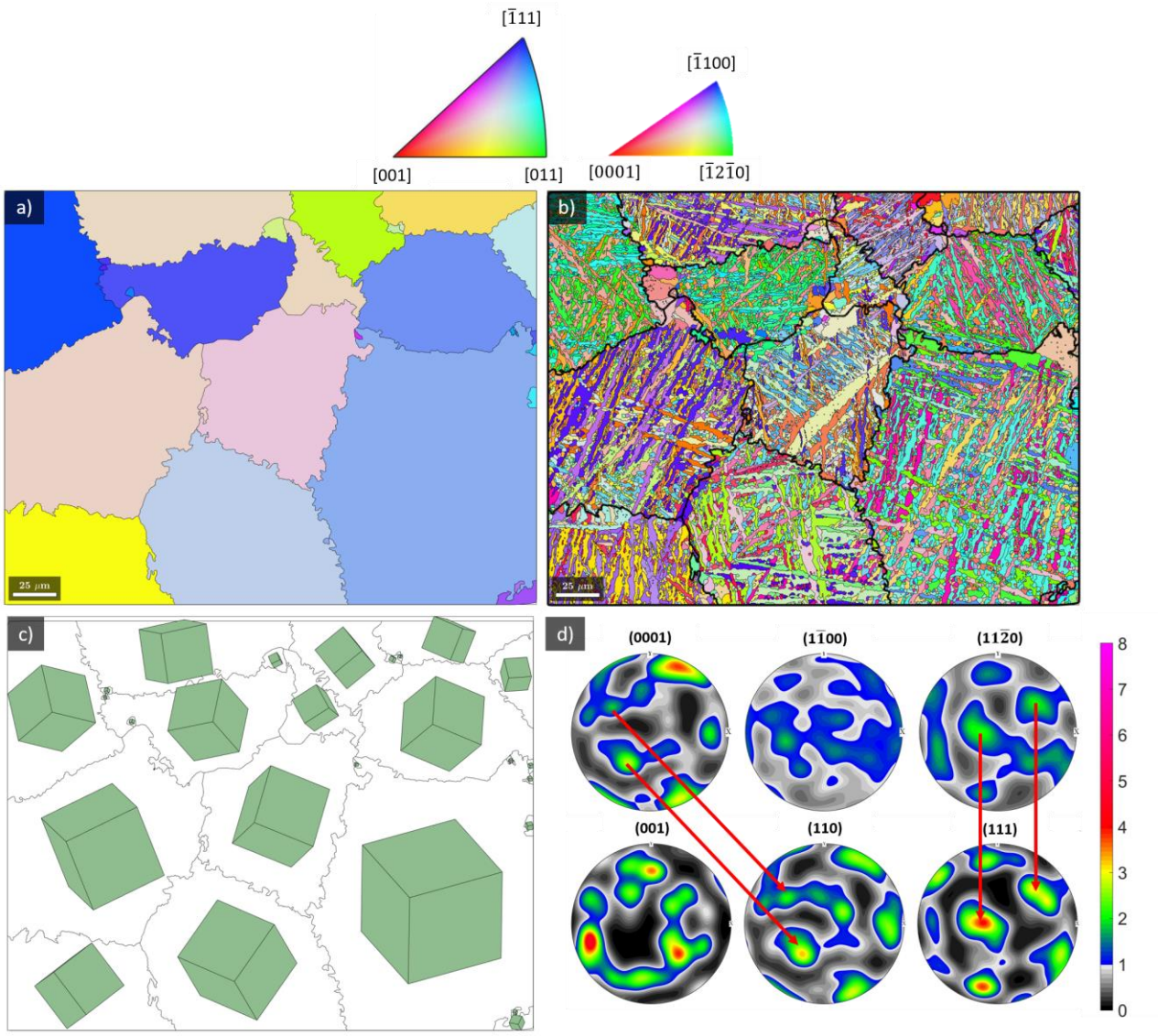

Figure 4: a) Reconstructed β-Ti microstructure IPF map from α' martensite assuming the Burgers OR. b) Overlaid parent β-Ti grains on the product IPF map to confirm the accuracy of the reconstruction process. c) Crystal map of the parent β-Ti grains illustrating crystal orientation in three-dimensional space. d) Pole figures for the α' martensite (top) and reconstructed β-Ti (bottom). The overlap of the $(0001)_\alpha$ -- $(110)_\beta$ pole and the $(11\bar{2}0)_\alpha$ -- $(111)_\beta$ pole figures confirms the Burgers OR was present for this system. All IPF maps are colored with respect to the normal direction (out of the screen). All pole figures are plotted in the same reference frame as IPF maps, with normal direction (Z-axis) out of the page, X-axis to the right, and Y-axis up the page.

3.4 EBSD of Ti-Cu Eutectoid

With reconstruction of the parent β-Ti phase validated for a product α' martensite microstructure, the next step was to validate this process with a eutectoid microstructure. Figure 1b demonstrates prior β-Ti grain sizes should be similar to those found for the martensitic reconstruction (~ 75 μm). Figure 5 illustrates the EBSD data acquired to test this idea. All data was processed using the

same grain misorientation thresholds and ODF resolutions applied to the martensitic EBSD data. Few EBSD maps of lamellae Ti-Cu microstructures have been completed, and seldom at the scales completed in this work [23]. Similar investigations with pearlite in ferrous systems remain a challenge due to the fine features of the microstructure [28].

Phase mapping of the system indicated the resolved eutectoid microstructure consisted of 25 pct. Ti_2Cu and 75 pct. α-Ti (Figure 5a). Ti_2Cu may have constituted a greater phase fraction, but this would require even finer EBSD step sizes to resolve. The texture of the α-Ti phase appears to be mostly random in the IPF map (Figure 5b) as evidenced by the lack of one dominant orientation color. This mild texture is confirmed by inspecting the pole figures in Figure 5d which demonstrate max textures at 2-3x multiples of uniform random distribution (m.r.d.). Curiously the Ti_2Cu demonstrates some texturing of the (001) planes, potentially indicative of the ~ 50° preferential misorientation between α-Ti and Ti_2Cu (Figure 5c). When calculated, this misorientation corresponds crystallographically to $\{0001\}_\alpha \parallel \{103\}_{Ti_2Cu}$ and $< 11\bar{2}0 >_\alpha \parallel < 010 >_{Ti_2Cu}$. Such a crystallographic alignment is a rotation of crystallographic directions from Donthula et al.'s reported OR between α-Ti and Ti_2Cu [23]. The determination of this similar OR *directly* from the dataset demonstrates the ease with which such information can be extracted from EBSD data with softwares such as MTEX and ORTools. Such determinations have long been challenging, requiring extensive characterization work even less than a decade ago.

A weak alignment of the $\{0001\}_\alpha$ and $\{103\}_{Ti_2Cu}$ planes can be seen in Figure 5d along with the $\{11\bar{2}0\}_\alpha$ and $\{331\}_{Ti_2Cu}$ planes, suggesting some portions of the microstructure maintain Donthula et al.'s OR [23]. The m.r.d. of these regions is barely above 1x m.r.d. though, demonstrating the preference for this OR is fairly weak. The OR reported in this work may constitute a higher fraction of the interfacial orientations observed in this microstructure as a result, potentially due to a shift in the interfacial direction alignment due to faster cooling rates in forming the eutectoid lamellae. This is additionally supported by Figure 5c where other crystallographic misorientations appear with moderate frequency, suggesting other ORs may be present. However, minimal overlap of the $\{11\bar{2}0\}_\alpha$ and $\{010\}_{Ti_2Cu}$ planes is observed in Figure 5d, demonstrating that though this OR is the most favorable, it may be the most common OR by only a small margin. The presence of multiple or similar ORs in pearlitic Ti-Cu is also in line with that observed in ferrous pearlitic microstructures, where multiple ORs are known to operate [22].

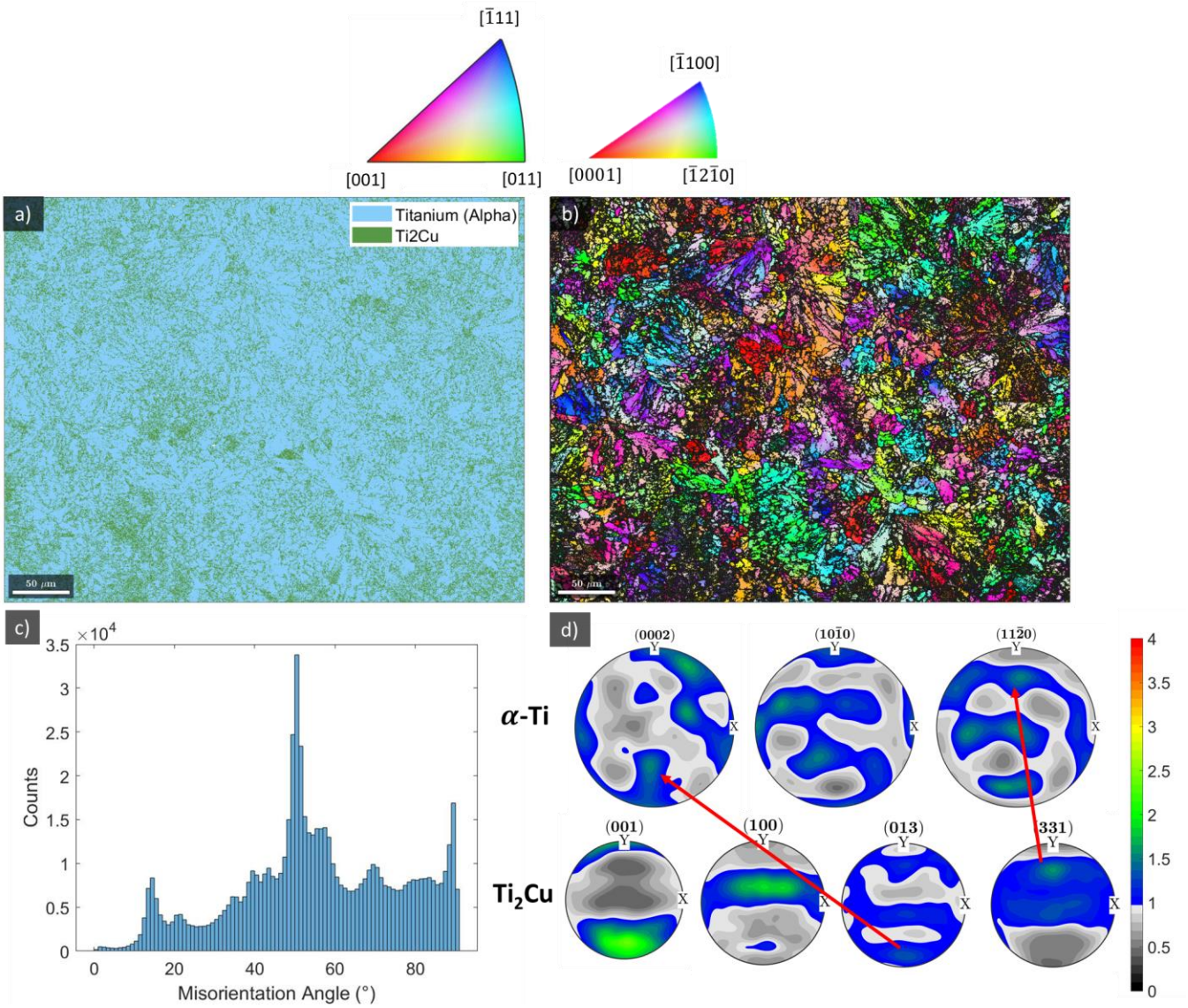

Figure 5: a) Phase map of the analyzed eutectoid microstructure. B) IPF map of the Ti_2Cu and α-Ti microstructure illustrating eutectoid colonies colored with respect to the normal direction (out of the page). C) Misorientation angle frequency between eutectoid α-Ti and Ti_2Cu phases in the eutectoid microstructure. D) Pole figures for the α-Ti(top) and Ti_2Cu (bottom) phases as calculated from the EBSD data. A weak overlap of the $\{0001\}_\alpha$ and $\{103\}_{Ti_2Cu}$ and $\{11\bar{2}0\}_\alpha$ and $\{331\}_{Ti_2Cu}$ planes is highlighted by the points connected by red arrows, indicating the potential presence of the previously reported OR between α-Ti and Ti_2Cu [23]. However, the weakness of the texture in this microstructure suggests other ORs are equally as likely or rotations of the reported OR are equally as preferred. All pole figures are plotted in the same reference frame as IPF maps, with normal direction (Z-axis) out of the page, X-axis to the right, and Y-axis up the page.

3.5 Reconstructing β-Ti Microstructures from Ti-Cu Eutectoid

With the previous OR between α-Ti and Ti_2Cu partially validated from the lamellae EBSD data, different reconstruction routes were implemented to reconstruct the parent β-Ti microstructure. Each route used the ORs identified here and by Donthula et al. [23] to form a single phase microstructure of either α-Ti or Ti_2Cu. Once one product phase was grown to dominate the whole microstructure, (thereby producing a single phase dataset analogous to the previous martensitic dataset), the respective OR with β-Ti (Burgers OR for α-Ti and $[001]_{Ti_2Cu}\| < 001 >_\beta$, $[100]_{Ti_2Cu}\| < 100 >_\beta$, and $[010]_{Ti_2Cu}\| < 010 >_\beta$ for Ti_2Cu) was implemented to reconstruct the parent grains. By creating a single-phase microstructure prior to reconstructing the parent β-Ti, the reconstruction process is greatly simplified. α-Ti or Ti_2Cu orientations can be grown to approximate the parent β-Ti grain volume they formed in, and then reconstructed using known ORs to determine the parent grain orientations.

It is also useful to note the reconstructed parent grain size should be the same as that recalculated for the α' martensitic microstructure. This is due to both specimens having the same trans-eutectoid temperature hold times, producing the same size of β-Ti grains prior to transformation. This acts as an easy metric to to distinguish if the reconstruction was accurate and successful. These two-step reconstruction processes were unsuccessful in reconstructing the parent β-Ti microstructures however. Implementing Donthula et al.'s OR for the α-Ti and Ti_2Cu [23] and the nearly equivalent form found in this work failed to create a single phase microstructure for simplified reconstruction. This is likely due to the lack of a dominant OR between the two product phases as previously discussed, meaning multiple ORs may be needed to successfully reconstruct the parent phase.

Reconstructions were also carried out on the as-scanned orientations of either the α-Ti or Ti_2Cu individually. The goal here was to take the true orientations of one phase without expanding it throughout the whole microstructure, and apply the respective OR with β-Ti to attempt reconstructions. Like with the two-step process however, this too could not produce reasonable reconstructed microstructures. Most surprising was the failure of β-Ti to be reconstructed from α-Ti using the Burgers OR, potentially indicative that this OR is not dominant in eutectoid microstructures at higher cooling rates in contrast to Donthula et al.'s findings [23].

Attempts to reconstruct the parent β-Ti microstructure with MTEX's triple point voting method also met with challenges, regardless of whether artificial single-phase datasets or the as-scanned data was used. From these tribulations however, a few important findings can be gleaned. It is likely the OR between α-Ti and Ti_2Cu discovered by Donthula et al. [23] is applicable to the pearlitic microstructure, and a form of this OR may in fact be the most frequent in the microstructure. The inability to reconstruct the eutectoid microstructure suggests this OR does not dominate the microstructure however, a fact also supported by the not-insignificant frequency of other ORs in Figure 5c and the low m.r.d. of coincident points in Figure 5d.

The inability to also implement the Burgers OR in *any* step of reconstruction on the pearlitic microstructure is in stark contrast to the ease in which the α' martensite microstructure was reconstructed. This demonstrates different crystallographic textures can be selectively triggered in Ti-Cu depending on the processing used to achieve solid state microstructures. This may have important applications in surface energy and wetting angle effects, especially regarding biomedical and antimicrobial performance of these alloys. Eutectoid, bainitic, and martensitic microstructures can all be achieved via conventional and AM processes, meaning the application space for these findings is potentially expansive.

4 Conclusions and Future Work

Through attempting to reconstruct parent β-Ti microstructures from pearlitic microstructures of eutectoid composition Ti-Cu, further insight into the ORs present in the solid state microstructure was developed. The alignment of crystallographic planes reported in other works was confirmed to be present in the material surveyed here as well. However, different direction vectors were identified, suggesting cooling rate may influence the OR of α-Ti + Ti_2Cu in eutectoid microstructures. The Burgers OR was not able to reconstruct any β-Ti from pearlitic microstructures despite previous work suggesting this OR is present in such microstructures with α-Ti. This is in stark contrast to other parts of this work, where the Burgers OR could accurately reconstruct β-Ti microstructures in eutectoid Ti-Cu consisting of α' martensite.

The ability to reconstruct the β-Ti microstructure for eutectoid composition Ti-Cu alloys is a valuable tool as the alloy system gains increasing adoption in engineering applications. The influence of processing in the β-Ti regime can be successfully understood (e.g, grain size in response to heat treatment or forging, crystallographic orientations, or abnormal grain growth) if the alloy is rapidly quenched to form a martensitically dominated microstructure. Though reconstructions are already used to evaluate the high temperature processing of other titanium and iron-based alloys, this was the first investigation to prove such a process can be implemented for binary Ti-Cu.

Ti-Cu alloys would benefit from the development of algorithms able to reconstruct parent microstructures with multiple competing ORs. This area of future work has considerable potential in not just Ti-Cu where pearlitic microstructures readily form, but also in ferrous alloys with pearlitic microstructures where multiple ORs are also present [22]. High temperature processing of ferrous alloys could then be easily inferred from pearlitic microstructures, instead of solely relying on information extracted from martensitic, bainitic, or allotriomorph dominated microstructures. Development of such a reconstruction algorithm is recommended, along with investigations into pearlitic Ti-Cu to identify what other ORs are present, preferably with even larger datasets than that surveyed here.

Acknowledgements

AIS would like to acknowledge the National Science Foundation (NSF) Graduate Research Fellowship Program (GRFP), USA, under Grant No. 2019260337 for support. AIS and AJC gratefully acknowledge the U.S. DOE, Office of Basic Energy Sciences, Division of Materials Sciences, Award No. DE-SC0020870 for supporting the experiments and analyses. AIS and AJC also thank the Center for Advanced Non-Ferrous Structural Alloys (CANFSA), USA, a National Science Foundation Industry/University Cooperative Research Center (I/UCRC), [Award No. 1624836] at the Colorado School of Mines (Mines), USA, for support completing this work. Scanning electron microscopy was supported by the NSF through DMR-1828454. AIS would also like to thank Dr. Adam Creuziger (National Institute of Standards and Technology) for previous guidance on understanding crystallographic texture, Dr. Adam Pilchak and Dr. Lee Semiatin (Air Force Research Laboratory) for help in understanding parent phase reconstructions, and Dr. Robert Field (Colorado School of Mines) for their help in proofing this work.

Data Availability

The raw/processed data required to reproduce these findings cannot be openly shared at this time as the data also forms part of an ongoing study. Reasonable requests for the data can be made to the corresponding author in the meantime.

References

[1] F. Niessen, T. Nyyssönen, A.A. Gazder, R. Hielscher, ArXiv:2104.14603 [Cond-Mat] (2021).
[2] M. Abbasi, T.W. Nelson, C.D. Sorensen, L. Wei, Materials Characterization 66 (2012) 1–8.
[3] A.I. Saville, S.C. Vogel, A. Creuziger, J.T. Benzing, A.L. Pilchak, P. Nandwana, J. Klemm-Toole, K.D. Clarke, S.L. Semiatin, A.J. Clarke, Additive Manufacturing 46 (2021) 102118.
[4] P.L. Stephenson, N. Haghdadi, R. DeMott, X.Z. Liao, S.P. Ringer, S. Primig, Additive Manufacturing 36 (2020) 101581.
[5] A.E. Davis, A. Caballero, P.B. Prangnell, Materialia 13 (2020) 100857.
[6] A.J. Clarke, R.D. Field, R.J. McCabe, C.M. Cady, R.E. Hackenberg, D.J. Thoma, Acta Materialia 56 (2008) 2638–2648.
[7] A.J. Clarke, R.D. Field, P.O. Dickerson, R.J. McCabe, J.G. Swadener, R.E. Hackenberg, D.J. Thoma, Scripta Materialia 60 (2009) 890–892.
[8] C. Cayron, J Appl Crystallogr 40 (2007) 1183–1188.
[9] C. Cayron, B. Artaud, L. Briottet, Materials Characterization 57 (2006) 386–401.
[10] A.L. Pilchak, J.C. Williams, Metallurgical and Materials Transactions A 42 (2011) 773–794.
[11] F. Bachmann, R. Hielscher, H. Schaeben, Solid State Phenomena 160 (2010) 63–68.
[12] A.F. Brust, E.J. Payton, T.J. Hobbs, S.R. Niezgoda, Microsc Microanal 25 (2019) 924–941.
[13] R. Hielscher, T. Nyyssönen, F. Niessen, A.A. Gazder, ArXiv:2201.02103 [Cond-Mat] (2022).
[14] D. Zhang, D. Qiu, M.A. Gibson, Y. Zheng, H.L. Fraser, D.H. StJohn, M.A. Easton, Nature 576 (2019) 91–95.
[15] Y. Alshammari, F. Yang, L. Bolzoni, Journal of the Mechanical Behavior of Biomedical Materials 95 (2019) 232–239.
[16] W. Zhang, S. Zhang, H. Liu, L. Ren, Q. Wang, Y. Zhang, Journal of Materials Science & Technology (2021) S1005030221002255.
[17] M. Takahashi, K. Sato, G. Togawa, Y. Takada, JFB 13 (2022) 263.
[18] C. Xin, N. Wang, Y. Chen, B. He, Q. Zhao, L. Chen, Y. Tang, B. Luo, Y. Zhao, X. Yang, Materials & Design 215 (2022) 110540.
[19] S.A. Souza, C.R.M. Afonso, P.L. Ferrandini, A.A. Coelho, R. Caram, Materials Science and Engineering: C 29 (2009) 1023–1028.
[20] J.C. Williams, R. Taggart, D.H. Polonis, MT 1 (1970) 2265–2270.
[21] G.W. Franti, J.C. Williams, H.I. Aaronson, MTA 9 (1978) 1641–1649.
[22] M.A. Mangan, G.J. Shiflet, Metall and Mat Trans A 30 (1999) 2767–2781.
[23] H. Donthula, B. Vishwanadh, T. Alam, T. Borkar, R.J. Contieri, R. Caram, R. Banerjee, R. Tewari, G.K. Dey, S. Banerjee, Acta Materialia 168 (2019) 63–75.

[24] R.J. Contieri, E.S.N. Lopes, R. Caram, A. Devaraj, S. Nag, R. Banerjee, Philosophical Magazine 94 (2014) 2350–2371.
[25] A.O.F. Hayama, P.N. Andrade, A. Cremasco, R.J. Contieri, C.R.M. Afonso, R. Caram, Materials & Design 55 (2014) 1006–1013.
[26] E04 Committee, Test Methods for Determining Average Grain Size, ASTM International, n.d.
[27] D.A. Porter, K.E. Easterling, Phase Transformation in Metals and Alloys, Third, Routledge, 2009.
[28] A. Walentek, M. Seefeldt, B. Verlinden, E. Aernoudt, P. Van Houtte, J Microsc 224 (2006) 256–263.